ELSEVIER

PII: S0266-3538(96)00125-X

Composites Science and Technology 57 (1997) 155-164

0266-3538/97/$17.00

MECHANICAL BEHAVIOUR OF ±55° FILAMENT-WOUND GLASS-FIBRE/EPOXY-RESIN TUBES: II. MICROMECHANICAL MODEL OF DAMAGE INITIATION AND THE COMPETITION BETWEEN DIFFERENT MECHANISMS

Jinbo Bai, Gengkai Hu & Philippe Bompard

Lab. MSS/MAT, CNRS URA 850, Ecole Centrale de Paris, 92295 Châtenay Malabry Cedex, France

(Received 15 April 1996; accepted 25 July 1996)

Abstract

This series of papers on ±55° filament-wound glass-fibre/epoxy-resin tubes consists of three parts. In the present paper (Part II), micromechanical modelling of the damage initiation is conducted in order to determine (1) the mechanical conditions under which different microcracking mechanisms occur and (2) the critical $\sigma_{zz}/\sigma_{\theta\theta}$ ratios which correspond to the change from interfacial failure to microcracking at porosity. Emphasis is placed on assessing the influence of microstructural defects and the competition between the different mechanisms. The general tendency of damage-envelope prediction by means of micromechanical modelling fits the microscopy observations quite well. The sensitivity of local criteria is also discussed. The correction of the local stress field has been improved by introducing a local stress concentration factor in a mean field theory model (Mori–Tanaka theory).

In Part I, the microstructural analyses, mechanical behaviour and damage initiation mechanisms were presented. In Part III, the macroscopic behaviour of the tubing structure with and without damage will be presented. The simulation results will be compared with experimental ones.

Keywords: composite tube, micromechanical modelling, mean field theory, porosity, damage initiation, transverse cracking, delamination, interfacial sliding and debonding

1 INTRODUCTION

Composite tubular elements are utilised as uniaxial structural components in several applications, such as mobile bridging components which have the advantages of easy transportation and *in situ* assembly,[1] supporting struts and pull in helicopters,[2] and trusses for satellites.[3] In these cases, cost saving per unit weight is of major consideration. Owing to the high resistance of composite materials in corrosive environments, composite pipelines have been used extensively for transferring fluids.[4–9] These pipelines are usually made of filament-wound fibre-reinforced polymer-matrix composites. For economic reasons, the fibres are often made of glass while the resin is usually a thermoset such as epoxy. Recent applications of the glass-fibre-reinforced composite tubular vessels in high-pressure and high axial loading operations have led to serious concerns about their functional and structural load-bearing behaviour. The leakage failure of a filament-wound fibre-composite vessel, subjected to a combined internal pressure and axial loading, is commonly viewed as a result of progressive damage produced by the coalescence of microcracks, thus creating a through-thickness crack path prior to complete loss of the tube's structural load-bearing capability. The nature of the problem is very complicated, since it involves the initiation and accumulation of various damage mechanisms in a heterogeneous and anisotropic medium under complex loading conditions.

Extensive experimental investigations have been conducted,[4–9] most of the studies being directed towards the prediction of failure envelopes for thin-walled cylinders with only a few wound layers. It was observed that tubes tested under biaxial failure loading conditions failed with greatly varying strengths, subsequently producing asymmetric biaxial failure envelopes (a biaxial failure envelope is a graph of the axial failure strength versus the circumferential failure strength). The failure envelopes depend strongly on the winding angles. It is generally recognised that a filament-wound tube with a winding angle of ±55° exhibits a higher strength under combined loading conditions.[4–6] Microscope observations for failure mechanisms of filament-wound composite tubes under combined load have been conducted by Jones and Hull,[10] Carroll *et al.*[5] and Bai *et al.*[11] In general, microcracking and delamination were the most readily observed damage mechanisms and any combination of the two constituted most failures. Two types of microcracking were established, notably cracking transverse to the fibre direction (transverse cracking) and cracking perpendicular to the loading direction in the resin-rich zones (matrix cracking). Transverse cracking is initiated at or near the fibre/matrix interface or/and at existing porosity and propagates through the ply thickness. This damage mode is more frequently observed in the region dominated by axial loading.[5,11] In the region dominated by internal pressure loading, delamination is the main damage mode.[5,6,11] It occurs more often between two adjacent layers. Prior to delamination, whitening of the tube is commonly observed.

The most likely damage initiation sites are the fibre/matrix interface and the microstructural defects.[11] The most frequently observed microstructural defects in this kind of composite structure are inter- and intra-ply porosity in the matrix, non-uniform fibre distribution (local fibre volume fraction fluctuation and inter-layer fibre-free resin layer) and fibre deviation away from the $\pm\theta$ alignment. It has been stated that there are fibre/interface/matrix interactions and interactions between layers which have a dominant effect on the early stages of mechanical failure, namely on damage (microcracking and delamination) initiation. The determination of local mechanical conditions depends on the knowledge of the local stress field and the interface strength which is in general not very well known.[12]

In our study, we consider a composite tube designed to transfer fluid for the cooling water, monitoring and fire systems in nuclear power stations. The tube is made of six plies with stacking sequence $[55°/-55°]_3$. Each laminate contains 56% glass fibre and the rest is epoxy resin. In the first paper (Part I),[11] the microstructural characteristics, stress/strain behaviour and damage mechanisms under pure tensile loading, pure internal pressure, and combined loading were investigated. Observations were made on these specimens in order to identify the damage initiation mechanisms and the effect of microstructural defects. In the third paper (Part III),[13] the macroscopic behaviour of the tube with and without damage will be presented. In the present paper, the competition between different mechanisms and the effect of a number of important factors will be discussed. First a micromechanical analysis is proposed. Construction of the failure envelope of the composite tube from a microscopic viewpoint will then be presented.

2 MICROMECHANICAL MODELLING

2.1 Coordinate systems

A number of plies constitute the composite tube in question, each one considered as a transverse isotropic material. An analytical method and a three-dimensional (3D) finite element calculation are presented elsewhere to evaluate 'mesoscopic' stress (on the scale of individual plies).[13,14] In order to characterise precise local damage modes and their causes, local stress fields at the scale of the fibres, the matrix, the interface and the voids are necessary. In the following section, a micromechanical model will be presented in local coordinates where the fibre axis is taken as x'_1. The local coordinate system x'_1, x'_2, x'_3 together with the composite tube's global reference system (x_1, x_2, x_3) are shown in Fig. 1.

Stress transformation from the global reference system to the local one is realised with the help of the following relationship:

$$\begin{bmatrix} \Sigma'_{11} \\ \Sigma'_{22} \\ \Sigma'_{33} \\ \Sigma'_{22} \\ \Sigma'_{13} \\ \Sigma'_{12} \end{bmatrix} = \begin{bmatrix} 0 & \cos^2\theta & \sin^2\theta & 2\sin\theta\cos\theta & 0 & 0 \\ 0 & \sin^2\theta & \cos^2\theta & -2\sin\theta\cos\theta & 0 & 0 \\ 1 & 0 & 0 & 0 & 0 & 0 \\ 0 & 0 & 0 & 0 & \cos\theta & -\sin\theta \\ 0 & 0 & 0 & 0 & \sin\theta & \cos\theta \\ 0 & -\sin\theta\cos\theta & \sin\theta\cos\theta & \cos^2\theta-\sin^2\theta & 0 & 0 \end{bmatrix} \begin{bmatrix} \Sigma_{11} \\ \Sigma_{22} \\ \Sigma_{33} \\ \Sigma_{23} \\ \Sigma_{13} \\ \Sigma_{12} \end{bmatrix} \quad (1)$$

Stresses obtained from tubular structure stress-state analysis are expressed in the global reference system[13,14] and they can be readily transformed into a local one by the previous transformation relation. The stresses expressed in the local reference system will be used for local stress analysis.

2.2 Mori–Tanaka micromechanical model

The Mori–Tanaka micromechanical model[15] takes into account the basic assumption that, for a composite under an external load, the stresses in an inclusion can be calculated approximately as the stresses round an inclusion embedded in an infinite matrix under remote matrix average stress loading. In

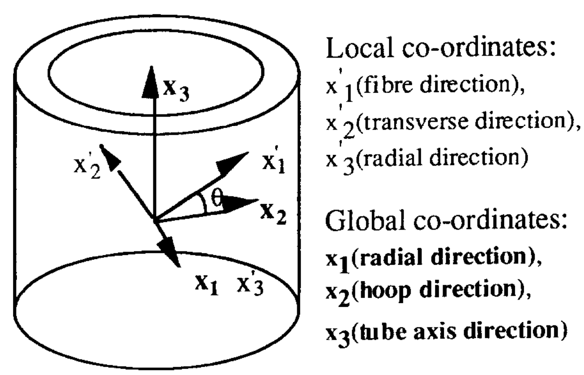

Fig. 1. Local and global reference systems.

the following formulation, fibres are assumed to be well aligned in the x_1' direction. $\boldsymbol{L}_0$,$\boldsymbol{L}_1$ denote the stiffness tensors of the matrix and the fibres, respectively (bold symbols represent a tensor). f is the fibre volume fraction for the composite under consideration and α is the aspect ratio.

Taking the matrix as a reference material under applied stress Σ', its strain will be $\boldsymbol{E}_0$ and $\Sigma' = \boldsymbol{L}_0\boldsymbol{E}_0$. For the composite under the same load, the average matrix strain will differ from $\boldsymbol{E}_0$ by $\bar{\epsilon}$. Thus the average stress in the matrix (for the composite) is given by $\sigma_{\mathrm{m}} = \boldsymbol{L}_0(\boldsymbol{E}_0 + \bar{\epsilon})$. The average strain in the fibre further differs from that in the surrounding matrix by ϵ^{pr}, so the average stresses inside the fibres are

$$\sigma_1 = \boldsymbol{L}_1(\boldsymbol{E}_0 + \bar{\epsilon} + \epsilon^{\mathrm{pr}}) \quad (2)$$

With aid of the Eshelby transformation method,[16] eqn (1) can be rewritten as

$$\sigma_1 = \boldsymbol{L}_1(\boldsymbol{E}_0 + \bar{\epsilon} + \epsilon^{\mathrm{pr}}) = \boldsymbol{L}_0(\boldsymbol{E}_0 + \bar{\epsilon} + \epsilon^{\mathrm{pr}} - \epsilon^*) \quad (3)$$

and we have the following Eshelby relationship:

$$\epsilon^{\mathrm{pr}} = \Pi\epsilon^* \quad (4)$$

where Π is the Eshelby tensor (see Appendix A).

For a representative volume under homogeneous loading conditions, the following relation is valid

$$\langle\sigma\rangle = \Sigma' \quad (5)$$

which leads to

$$\bar{\epsilon} + f(\epsilon^{\mathrm{pr}} - \epsilon^*) = 0 \quad (6)$$

From the above equations, we can determine the unknown quantities $\bar{\epsilon}$, ϵ^{pr} and ϵ^*. The eigenstrain ϵ^* can be expressed as

$$\epsilon^* = -\boldsymbol{Q}(\boldsymbol{I} + \boldsymbol{N})\boldsymbol{L}_0^{-1}\Sigma' \quad (7)$$

where

$$\boldsymbol{Q} = [(\boldsymbol{L}_0 - \boldsymbol{L}_1)\Pi - \boldsymbol{L}_0]^{-1}(\boldsymbol{L}_0 - \boldsymbol{L}_1)$$

and

$$\boldsymbol{N} = [\boldsymbol{I} - f(\Pi - \boldsymbol{I})\boldsymbol{Q}]^{-1}f(\Pi - \boldsymbol{I})\boldsymbol{Q}$$

The average stresses in the matrix and in the fibre are

$$\sigma_{\mathrm{m}} = \boldsymbol{L}_0(\boldsymbol{I} + \boldsymbol{N})\boldsymbol{L}_0^{-1}\Sigma' \quad (8)$$

$$\sigma_1 = \boldsymbol{L}_0[(\boldsymbol{I} - (\Pi - \boldsymbol{I})\boldsymbol{Q})(\boldsymbol{I} + \boldsymbol{N})]\boldsymbol{L}_0^{-1}\Sigma' \quad (9)$$

Finally, the compliance tensor of the composite is calculated by

$$\boldsymbol{S}_{\mathrm{c}} = [\boldsymbol{I} - f\boldsymbol{Q}(\boldsymbol{I} + \boldsymbol{N})]\boldsymbol{L}_0^{-1} \quad (10)$$

The stress at the interface just outside the fibres can be expressed as:[17]

$$\sigma_{ij}^{in} = \sigma_{ij}^{1} + L_{ijkl}^{0}[L_{pqmn}^{0}\epsilon_{mn}^{*}M_{kp}n_q n_l + \epsilon_{kl}^{*}] \quad (11)$$

where $M_{kp} = 1/\mu_0[\delta_{kp} - n_k n_p/2(1 - \nu_0)]$ and $\vec{n}$ is the normal vector to the matrix/fibre interface.

In the $x_1'x_2'$ plane, the normal vector is $\vec{n} = \{\sin\xi, \cos\xi, 0\}$ (see Fig. 2), and $\tan\varphi = \alpha^2\tan\xi$. In this case, eqn (11) can be simplified as follows:

$$\sigma_{11}^{in} = \sigma_{11}^{1} + \frac{2\mu_0}{1-\nu_0}[\cos^2\xi(\epsilon_{11}^{*}\cos^2\xi + \epsilon_{22}^{*}\sin^2\xi + \nu_0\epsilon_{33}^{*}) - 2\epsilon_{12}^{*}\sin\xi\cos^3\xi]$$

$$\sigma_{22}^{in} = \sigma_{22}^{1} + \frac{2\mu_0}{1-\nu_0}[\sin^2\xi(\epsilon_{11}^{*}\cos^2\xi + \epsilon_{22}^{*}\sin^2\xi + \nu_0\epsilon_{33}^{*}) - 2\epsilon_{12}^{*}\sin^3\xi\cos\xi]$$

$$\sigma_{33}^{in} = \sigma_{33}^{1} + \frac{2\mu_0}{1-\nu_0}[\nu_0(\epsilon_{11}^{*}\cos^2\xi + \epsilon_{22}^{*}\sin^2\xi) + \epsilon_{33}^{*} - 2\nu_0\epsilon_{12}^{*}\sin\xi\cos\xi]$$

$$\sigma_{23}^{in} = \sigma_{23}^{1} + 2\mu_0[\epsilon_{23}^{*}\sin^2\xi - \epsilon_{13}^{*}\sin\xi\cos\xi]$$

$$\sigma_{13}^{in} = \sigma_{13}^{1} + 2\mu_0[\epsilon_{13}^{*}\sin^2\xi - \epsilon_{23}^{*}\sin\xi\cos\xi]$$

$$\sigma_{12}^{in} = \sigma_{12}^{1} + \frac{2\mu_0}{1-\nu_0}\sin\xi\cos\xi[-(\epsilon_{11}^{*}\cos^2\xi + \epsilon_{22}^{*}\sin^2\xi + \nu_0\epsilon_{33}^{*}) + 2\epsilon_{12}^{*}\sin\xi\cos\xi]$$

Projections of this interfacial stress along and perpendicular to the normal $\vec{n}$ give us the normal stress and shear stress at the interface between the matrix and the fibre. These lead to

$$\sigma_{\mathrm{n}} = \sigma_{11}^{in}\sin^2\xi + \sigma_{22}^{in}\cos^2\xi + 2\sigma_{12}^{in}\sin\xi\cos\xi \quad (12)$$

and

$$\tau = \sqrt{T_1^2 + T_2^2 - \sigma_{\mathrm{n}}^2} \quad (13)$$

where

$$T_1 = \sigma_{11}^{in}\sin\xi + \sigma_{12}^{in}\cos\xi$$

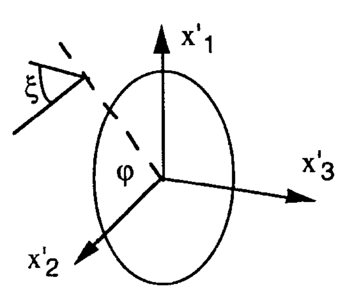

Fig. 2. Definition of the normal vector at the interface.

and

$$T_2 = \sigma_{12}^{in} \sin \xi + \sigma_{22}^{in} \cos \xi$$

The normal and shear stresses can be further simplified by putting the interfacial stresses into eqns (12) and (13). They are

$$\sigma_n = \tfrac{1}{2}[\sigma_{11}^1 + \sigma_{22}^1 - (\sigma_{11}^1 - \sigma_{22}^1)\cos 2\xi + 2\sigma_{12}^1 \sin 2\xi]$$

and

$$\tau = \tfrac{1}{2} 2\sigma_{12}^1 \cos 2\xi + \sigma_{11}^1 \sin 2\xi - \sigma_{22}^1 \sin 2\xi$$

If one considers the influence of the voids in an individual ply on the stress field, the previous method can be extended to include this effect. Let f_v denote the void volume fraction in the ply under consideration. The voids are all considered as ellipsoidal cavities with the same aspect ratio, α_1. The previous micromechanical formulation remains the same except for the expressions of $\boldsymbol{N}$ and the composite's compliance tensor, which assume the following forms:

$$\boldsymbol{N} = \{(1 - f_v)\boldsymbol{I} - f(\Pi_1 - \boldsymbol{I})\boldsymbol{Q}\}^{-1}\{f_v \boldsymbol{I} + f(\Pi_1 - \boldsymbol{I})\boldsymbol{Q}\} \quad (14)$$

and

$$\boldsymbol{S}_c = \{\boldsymbol{I} - f\boldsymbol{Q}(\boldsymbol{I} + N) - f_v(\Pi_1 - \boldsymbol{I})^{-1}(\boldsymbol{I} + \boldsymbol{N})\}\boldsymbol{S}_0 \quad (15)$$

The eigenstrain for the voids is expressed as:

$$\epsilon^{*1} = -(\Pi_1 - \boldsymbol{I})^{-1}(\boldsymbol{I} + \boldsymbol{N})\boldsymbol{L}_0^{-1}\Sigma'$$

Eshelby's tensor for voids Π_1 is calculated by using a void aspect ratio. Stresses just outside voids can be obtained by the same method as described for fibres. With the help of the previous micromechanical model, the elastic constants of each individual ply can also be predicted. For the composite studied, the fibre volume fraction is $f = 0{\cdot}56$, and the elastic constants for the matrix and the fibre are $E_m = 3{\cdot}4$ GPa, $\nu_m = 0{\cdot}35$; $E_f = 73{\cdot}8$ GPa, $\nu_f = 0{\cdot}23$, respectively. The predicted elastic constants of the laminate are: $E_l = 42{\cdot}84$ GPa, $E_t = 10{\cdot}13$ GPa, $G_{lt} = 3{\cdot}93$ GPa, $G_{tt} = 3{\cdot}50$ GPa, $\nu_{lt} = 0{\cdot}2758$ and $\nu_{tt} = 0{\cdot}4467$. These constants are used to calculate the stress distributions in the composite tube under different loading conditions.

2.3 Local interfacial stresses in the internal ply of the composite tube

Finite-element and analytical calculations conducted for a filament-wound composite tube under pure tension and internal pressure show that the internal ply is under more stress than the other plies.[13,14] Consequently, we shall use the stresses in the internal ply obtained by an analytical calculation as input for evaluating interfacial stresses (normal and shear) and stresses at the porosity. With the help of these stresses, we expect to derive a local damage criterion for this ply, and following that the critical external loads which can be applied on the composite tube.

Table 1. Stresses in the internal ply under pure tension ($F = 10$ kN) expressed in local coordinates

σ_{11}	σ_{22}	σ_{33}	σ_{23}	σ_{13}	σ_{12}
11·5	8·6	20·4	0	0	−10·4

Table 2. Stresses in the internal ply under pure internal pressure ($p = 10$ MPa) expressed in local coordinates

σ_{11}	σ_{22}	σ_{33}	σ_{23}	σ_{13}	σ_{12}
120	−2·3	−10	0	0	42

For a pure tension and a pure internal pressure load, the corresponding stresses in the internal ply are shown in Tables 1 and 2. The local stresses for the composite tube loaded under different conditions are now presented.

2.3.1 Composite tube loaded in pure tension (unit stress)

The local stress fields at the interface and around the porosity in the internal ply were obtained by using the above theory and the data in Table 1 (see Fig. 3). It can be seen that the porosity is much more stressed under global tensile loading. Microcracks should be initiated from the porosity first. That was what has been identified as the first damage mechanism.[11]

An increase of void volume fraction to 0·10 gives an increase of about 10% in the local stresses, corresponding to the average effect predicted by the Mori–Tanaka theory.

2.3.2 Composite tube under pure internal pressure loading

The local stress fields at the interface and the porosity in the internal ply were obtained by using the above theory and the data in Table 2 (see Fig. 4). It can be seen that it is the interface that is much more stressed under global pure internal pressure loading. Microcracks should be initiated first at the interface by shear stress. Neither microcracking initiated at voids nor debonding at the interface by normal stress should be observed, because they are in low-level compression. These conclusions agree very well with the damage micromechanism observations.[11] Apart from a few matrix cracks in the resin-rich zones, the first damage mechanism observed was delamination. No transverse cracking was noticed. In fact, in the case of filament-wound tubes, sliding at the interface is not possible owing to the structural constraint in this kind of tube. It can be observed only in the resin-rich zones and in the zones where the fibres are misaligned or discontinuous. This kind of damage (sliding at the interface), however, could reduce the shear modulus in a certain direction of the composite tubes.

2.3.3 Composite tube under combined loading

Figure 5 shows the influence of the $\sigma_{zz}/\sigma_{\theta\theta}$ ratio on the local stress distribution. The maximum stress near

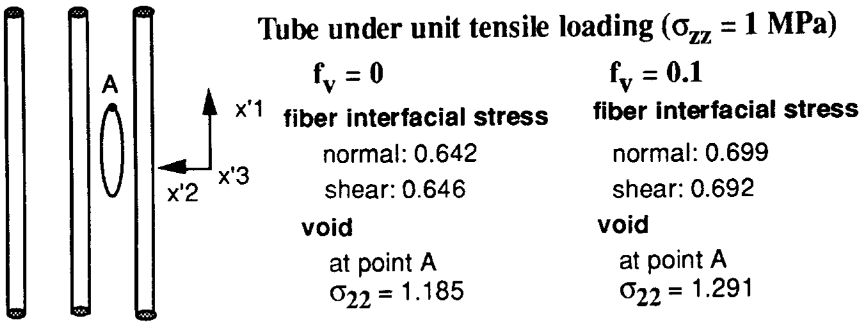

Fig. 3. Local stress fields in the internal ply and influence of the voids under pure tension loading expressed in local coordinates.

voids and the normal interfacial stress increase as a function of $\sigma_{zz}/\sigma_{\theta\theta}$. Interfacial shear stress, however, decreases until a certain ratio of $\sigma_{zz}/\sigma_{\theta\theta}$ and then increases. A change of the first damage initiation mechanism, from interfacial shear-stress-activated damage to cracking at porosity, takes place when the $\sigma_{zz}/\sigma_{\theta\theta}$ ratio increases. The exact value of this ratio depends on the local fracture criteria. It can also be seen that the average influence of the volume fraction of porosity (f_v) is very small. It becomes noticeable around the voids only for a very high $\sigma_{zz}/\sigma_{\theta\theta}$ ratio.

3 FAILURE PREDICTION OF A PLY BY MICROMECHANICAL MODELLING

In the previous sections, we applied a mean-field (Mori–Tanaka) theory of micromechanics to determine the elastic constants of each ply, the local average stress in different phases and the local stress fields at the interface and around the voids. In this section, we discuss the strength of a composite tube on the local scale, that is at the scale of the interface between matrix and fibre and the defects (voids) in a critically loaded ply. Three local failure modes are investigated which enable us to study the competition between different damage mechanisms and to determine the corresponding critical macroscopic loads. The three failure criteria employed here are based on experimental observations,[11] corresponding to three damage mechanisms: (a) microcrack initiation from cavities (porosity); (b) crack initiation at the interface of matrix and fibre by interfacial shear stress; and (c) transverse ply cracking initiated at the interface by interfacial normal stress. By using these three local damage criteria, it is possible to determine the corresponding macroscopic applied loads. The method can be explained as follows. Under a given combined macroscopic load, the stress fields in each ply (analytical or finite-element methods) can be determined; then both the stresses near the voids, and normal and shear stresses along the interface in each ply can be evaluated by means of micromechanical methods. Subsequently we compare these local stresses with corresponding critical values and determine in this manner the strength of the composite tube. The following local values are chosen: $\sigma_{nc} = 80$ MPa, $\tau_c = 53{\cdot}3$ MPa; when the principle maximum stress near a void reaches 80 MPa, a crack will be initiated at this void; when the interfacial shear stress reaches 53·3 MPa, a crack will be initiated or sliding will take place at the interface; when the interfacial normal stress reaches 80 MPa, a crack will be initiated at the interface by debonding. The choice of 80 MPa for σ_{nc} was made after a uniaxial tensile test on pure resin specimens. The maximum value is considered as the fracture strength of the resin. There are no credible values for τ_c. Most probably, a ratio smaller than 2 should be used for σ_{nc}/τ_c: a value of 1·5 was used in this investigation.

For comparison, the microscope observation results are reported in Fig. 6(a).[11] Figure 6(b) shows the predicted results together with the experimental ones.

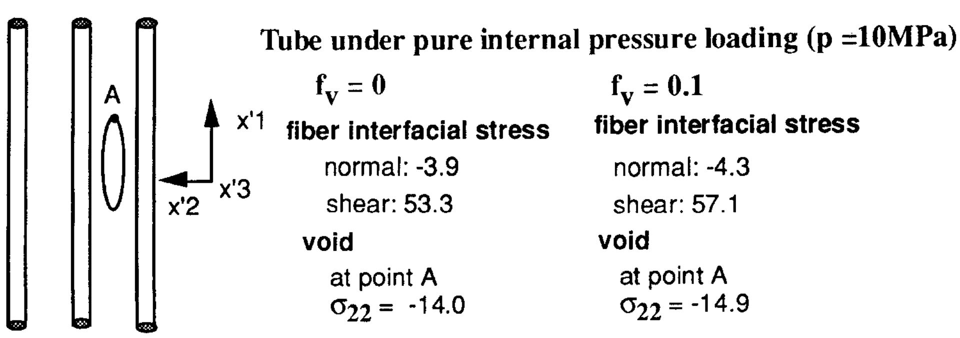

Fig. 4. Local stress fields in the internal ply and influence of the voids under pure internal pressure loading expressed in local coordinates.

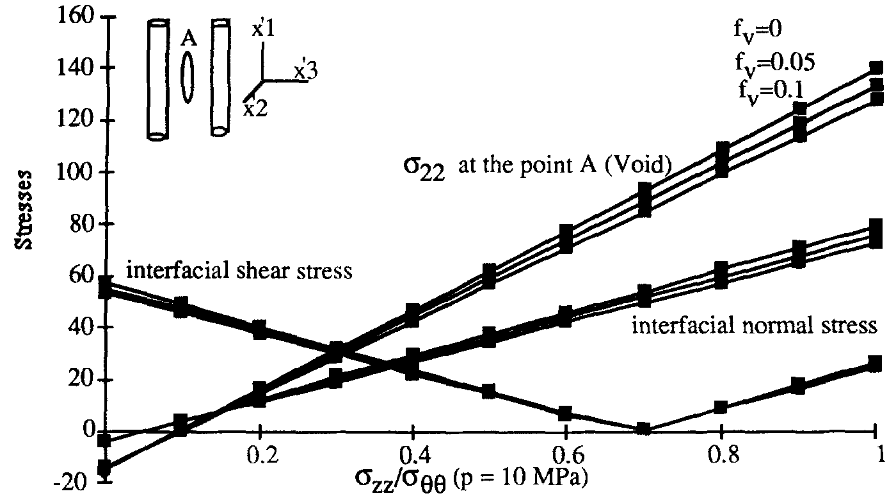

Fig. 5. Local stress fields in the internal ply and influence of the voids under combined loading expressed in local coordinates.

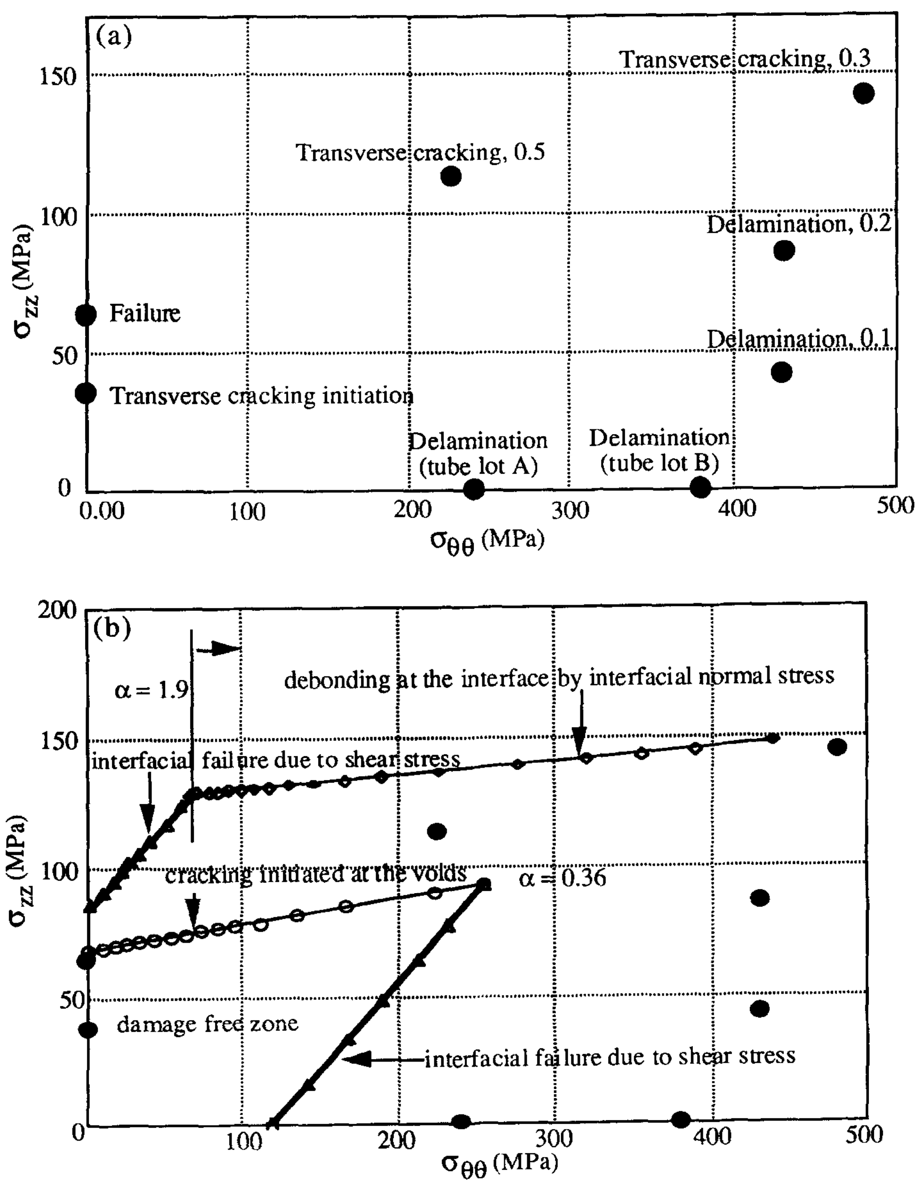

Fig. 6. (a) Stress envelope with damage mechanisms and failure modes for different $\sigma_{zz}/\sigma_{\theta\theta}$ ratios.[11] (b) Comparison between the micromechanical modelling and the experimental results (filled symbols).

It can be seen that in an internal-pressure-dominated region, the results predicted by the micromechanical approach are again conservative. The explanation for such a difference is not evident since, from a mesoscopic point of view, the predicted results have the same tendency (conservative prediction for the internal-pressure-dominated region).[13]

It should be mentioned that the delamination observed in this study is always of an inter-ply nature. It is not controlled directly by the stresses inside plies, but depends on the different deformation patterns inside two adjacent plies. As shown in Table 2,[13] strong in-plane shear stresses exist. They change sign when crossing the interface between two plies. This may be the origin of delamination, i.e. the incompatible shear strains between two plies. The thin resin layer between plies may be the preferred site for delamination initiation.[11,13]

4 DISCUSSION

4.1 Comparison with microscopical observations

The general tendency predicted by the micromechanical model agrees well with micromechanism observations presented in Part I[11] of this series of papers. The threshold stresses increase with increasing $\sigma_{zz}/\sigma_{\theta\theta}$ ratio. In the case of tensile loading, the first damage mechanism was matrix cracking, the cracks initiating at the zones free of fibres or at the outer resin skin. The second damage mechanism observed was transverse cracking, being located mainly in the vicinity of the porosity, indicating the strong effect of porosity on the damage initiation. In the case of internal pressure loading, apart from a few matrix microcracks observed in the external resin layer, for a higher stress level, delamination initiated either from the intra-ply matrix cracking or from the inter-ply porosity. Whitening was also observed on the outer skin of the tubes although few damage traces were found over a large area of examination.

According to the prediction of the micromechanical model, one should be able to observe, for a tensile test, cracks initiating at the porosity first for $\sigma_{zz} = 62$ MPa. Some kind of interfacial failure due to interfacial shear stresses should also be visible for a higher stress level.

In the case of internal pressure loading, interfacial sliding due to interfacial shear stresses would occur for $\sigma_{\theta\theta} = 120$ MPa. The explanation for the absence of this phenomenon in microscope observations on long tube specimens may reside in the constraint effect of symmetric filament-wound tubes. Sliding along the continuous fibres is either not possible or leaves no noticeable traces. This sliding might be also partially reversible owing to the viscous or elastic nature of the matrix. A special study is under progress at the moment which will help us to understand this phenomenon.[18] It can be concluded that this interfacial sliding occurred at a pre-polished free surface at about $\sigma_{\theta\theta} = -90$ MPa in compression and $\sigma_{\theta\theta} = 140$ MPa in hoop tensile tests. This observation indicates that the choice of $\tau_c = 53$ MPa for the local interfacial fracture criterion is relatively correct.

It should be also mentioned that observations of the fracture surfaces of the composite tubes revealed that the surfaces of pulled-out fibres were very smooth, indicating a relatively poor interfacial shear strength. This mechanism has little effect on the mechanical properties of the tube, being of very small scale and appearing not very frequently.

By contrast, for combined loading with $\sigma_{zz}/\sigma_{\theta\theta} > 1{\cdot}9$ another mechanism related to the interface failure is very detrimental to the composite tube behaviour, i.e. debonding by interfacial normal stress. The threshold stress is quite high and increases with $\sigma_{zz}/\sigma_{\theta\theta}$ ratio. The average effect results in numerous microcracks (one crack for one fibre). A continuous path can easily be created by these cracks which leads to weeping. The stress-transfer capacity of the fibres and the tube integrity may or may not deteriorate. The macroscopic loading level should be kept below a certain value above which there is still a margin before the local stress fields reach this fracture criterion.

A possible way of taking into account the effect of both of these two mechanisms is to reduce the corresponding modulus for each of them, i.e. reducing G_1 for interfacial shear stress damage and E_3 for interfacial normal stress damage.[13]

4.2 Effect of the choice of local criteria

In this study, values of $\sigma_{nc} = 80$ MPa and $\tau_c = 53{\cdot}3$ MPa were used as the local critical strengths and the absence of coupling of τ_c and σ_{nc} for the local fracture criteria. Physically, there would be some interaction effect between these two components, as in most cases. However, the experimental data are insufficient to qualify this. Asp *et al.*[19] concluded that uniaxial matrix strain to failure cannot generally be expected to correlate with initiation values of transverse strain to failure. Differences in the state of stress and the geometry of the problem will result in vastly different failure mechanisms. The poker-chip strains to failure in the primary loading direction were 0·5–0·8%, so the uniaxial stress state in composite matrices may therefore by itself be a sufficient explanation for low values of transverse composite strains to failure. Furthermore, an investigation of pressurised glass-fibre/polyester pipes provides an example of how transverse cracks form early in the deformation process of a composite structure.[20] Onset of weepage due to transverse cracks occurred at transverse strains of about 0·2% whereas final failure occurred much later. By contrast, Piggott[21] has recently proposed that with polymers which have extended covalently bonded structures, molecular disruption in shear is as difficult as it is in tension, and may well be activated by tension instead of shear. Subsequently the failure process in shear tests is almost certainly tension rather than shear. He then used a new model of fibre debonding from the matrix in a tensile failure fashion to explain the unusually high interfacial shear strengths in reinforced polymers.

From a quantitative point of view, the micromechanical prediction gave higher threshold stresses for first damage initiation (transverse cracking) than observations in principally tensile loading regions. Two explanations could be given, one is that the value of σ_{nc} was not correctly chosen. The second may be that the stress state effect was not correctly represented by the micromechanical model theory. To improve this prediction, tests under a similar stress state should be performed in order to determine the critical values for σ_{nc} and τ_c. Under internal pressure loading, only delamination was observed as a main damage mode at a stress level much higher than that for interfacial shear failure predicted by the micromechanical model. The plies are subjected to 3D loading with a very large in-plane shear stress, meaning shear along the fibre axis. This situation does not correspond to any known tests in the literature.

Here, values of $\sigma_{nc} = 64$ MPa and $\tau_c = 42$ MPa[21] and the structural stress-state analysis results in Tables 1 and 2 will be used. Higher $f_v = 0{\cdot}15$, and $K_{tc} = 1{\cdot}2$ are chosen to evaluate the influence of these parameters on the prediction. K_{tc} will only affect the interface failure. Figure 7 depicts the predicted results using the new parameters. For tensile loading, the predicted stress for debonding at the interface by interfacial normal stress is very close to the experimental fracture strength. The stress corresponding to first damage initiation (being 50 MPa), however, is still higher than the experimental values (about 30 MPa).

4.3 Effect of the number and volume fraction of voids (porosity)

The micromechanical model indicates that the average effect of an increase in the void volume fraction on the local stress field, proportionally increased, is small. A local mechanical effect of the porosity is the increase in the stress concentration at the interface. A complementary coefficient of stress concentration, K_{tc}, should be introduced to take this effect into account, because the micromechanical model gives only an average effect. By a 2D finite-element calculation, it was found that for $f_v = 0{\cdot}05$ and a cubic distribution of fibres and porosity, K_{tc} equals 1·2. This coefficient, larger than one, will still reduce the strength of the interface. The technical importance of this effect is that a void can affect the interface of fibres in its neighbourhood, showing again the detrimental effect of increasing the number of voids.

In practice, a detrimental effect of porosity is to provide more nucleation sites for microcracks and then to reduce the length of the propagation path before their coalescence. To obtain a quantitative description, the concept of the representative defect is used.[11] The value of $f_v = 0{\cdot}05$ means having one void in the ply thickness direction within a circumferential distance of about 625 μm in the case of ideal distribution. The propagation distance is reduced to 210 μm (half thickness). If f_v increases to 0·1, there may be two voids in the thickness direction (in the worst case), the propagation distance becoming 105 μm. From this point of view, a small size porosity of is more detrimental than a larger size one, for the same volume fraction. The present authors suggest a limit of f_v below 0·05 in order to avoid any possible detrimental effect.

In this study an aspect ratio of 15 was used for the porosity in the micromechanical modelling. The choice of this value is a result from an average over the microstructural analysis information. According to the microstructural analysis presented in Part I,[11] some of the voids have an aspect ratio larger than 15. The porosity is less stressed with a smaller aspect ratio. This enhancing effect, however, is stabilised for an aspect ratio larger than 14.

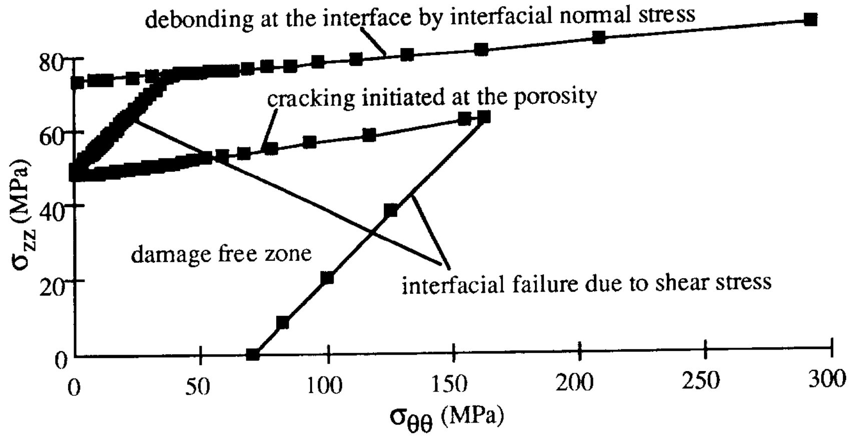

Fig. 7. Results predicted by the micromechanical model with new parameters.

5 CONCLUSIONS

A micromechanical model based on the Mori–Tanaka theory has been formulated which enables the determination of the local stress fields at the interface and at the porosity in a critically loaded ply of the studied composite tube. The general tendency of the threshold stresses predicted by the micromechanical model agrees well with the micromechanism observations presented in Part I[11] of this series of papers. The model can also provide useful information for correlating the microscale damage with the macroscopic behaviour of the tubes under combined loading. The porosity volume fraction should be kept below 0·05 to avoid any detrimental effect. There still remains some work to be done in order to improve the local criteria and the choice of critical stress values used in them.

ACKNOWLEDGEMENTS

The present research is supported by EDF-DER (Electricité de France). The authors are grateful to Drs F. Nagot, J. Le Bras and M. Lasne (EDF-MTC) and Professor D. François for valuable discussions, and Professor D. Baptiste (ENSAM, Paris) for initiating this project. The work was carried out in the laboratory MSS/MAT of Ecole Centrale Paris (CNRS URA 850). The authors would like to acknowledge the assistance rendered by their colleagues.

REFERENCES

1. Tsiang, T. H., Brooksstein, D. & Dent, J., Mechanical characterisation of braided graphite/epoxy cylinders. In *Proc. 29th National SAMPE Symposium*, April 1984, pp. 880–890.
2. Aker, S. C. & Sonneborn, W. G. O., Composite control tubes. In *Proc. 13th National SAMPE Technical Conf.*, October 1981, pp. 280–287.
3. Kawashima, T., Development of graphite/epoxy tube truss for satellite. In *Proc. Japan–US Conf. on Composite Materials*, Tokyo, 1981, pp. 453–459.
4. Karayaka, M., Srinivasan, S., Miyase, A. & Wang, S. S., Leakage damage and failure of glass-fibre reinforced composite tubular vessels under combined internal pressure and axial loading. In *Proc. 10th Int. Conf. on Composite Materials*, Whistler, BC, Canada, August 1995. Vol. I, pp. 747–754.
5. Carroll, M., Ellyin, F., Kujawski, D. & Chiu, A. S., The rate-dependent behaviour of ±55° filament-wound glass-fibre/epoxy tubes under biaxial loading. *Compos. Sci. Technol.*, **55** (1995) 391–403.
6. Hinton, M. J., Soden, P. D. & Kaddour, A. S., Strength of composite laminates under biaxial loads. In *Proc. 10th Int. Conf. on Composite Materials*, Whistler, BC, Canada, August 1995. Vol. IV, pp. 65–72.
7. Hull, D., Legg, M. J. & Spencer, B., Failure of glass/polyester filament wound pipe. *Composites*, **9** (1978) 17–24.
8. Soden, P. D., Leadbetter, D., Griggs, P. R. & Eckold, G. C., The strength of a filament wound composite under biaxial loading. *Composites*, **9** (1978) 247–250.
9. Foral, R. F. & Gilbreath, D. R., Delamination failure mode in filament wound composite tube. In *ASTM STP 1012*, American Society for Testing and Materials, Philadelphia, 1989, pp. 313–325.
10. Jones, M. L. C. & Hull, D., Microscopy of failure mechanisms in filament-wound pipe. *J. Mater. Sci.*, **14** (1979) 165–174.
11. Bai, J. B., Seeleuthner, Ph. & Bompard, Ph., Mechanical behaviour of ±55° filament-wound glass-fibre/epoxy-resin tubes: I. Microstructural analyses, mechanical behaviour and damage mechanisms of composite tubes under pure tensile loading, pure internal pressure, and combined loading. *Compos. Sci. Technol.*, **57** (1997) 141–153.
12. Bader, M. G., Bailey, J. E., Curtis, P. T. & Parvizi, A., The mechanisms of initiation and development of damage in multi-axial fibre-reinforced plastics laminates. In *Proc. 3rd Int. Conf. on Materials* (*ICM*-3), Cambridge, UK, August 1979, pp. 227–239.
13. Hu, G. K., Bai, J. B., Demyanushko, K. & Bompard, Ph., Mechanical behaviour of ±55° filament-wound glass-fibre/epoxy-resin tubes: III. Macromechanical modelling of the macroscopical behaviour of the tubing structure with damage effect and failure envelope prediction. *Compos. Sci. Technol.* (in press).
14. Demyanushko, K. & Bai, J. B., Local and global stress state analyses of a ±55° filament winding tube with damage effect. *Comp. Struct.* (submitted).
15. Mori, T. & Tanaka, K., Average stress in matrix and average elastic energy of materials with misfitting inclusions. *Acta Metall.*, **21** (1973) 591–594.
16. Eshelby, J. D., The determination of the elastic field of an ellipsoidal inclusion, and related problems. *Proc. Roy. Soc. Lond.*, **241A** (1957) 376–396.
17. Tandon, G. P. & Weng, G. J., Stress distribution in and around spheroidal inclusions and voids at finite concentration. *ASME J. Appl. Mech.*, **53** (1986) 511–518.
18. Dontchev, D., Bai, J. B., Djafari, V. & Bompard, Ph., Whitening phenomenon in a ±55° filament-wound glass-fibre/epoxy-resin tubes (to be published).
19. Asp, L. E., Berglund, L. A. & Gudmundson, P., Effects of a composite-like stress state on the fracture of epoxies. *Compos. Sci. Technol.*, **53** (1995) 27–37.
20. Spencer, B. & Hull, D., Effect of winding angle on the failure of filament wound pipe. *Composites*, **10** (1978) 263–271.
21. Piggott, M. R., A new model for interface failure in fibre-reinforced polymers. *Compos. Sci. Technol.*, **55** (1996) 269–276.

APPENDIX A

Components of Eshelby's tensor

$$\Pi_{1111} = \frac{1}{2(1-\nu_0)}\left\{1 - 2\nu_0 + \frac{3\alpha^2-1}{\alpha^2-1} - \left[1 - 2\nu_0 + \frac{3\alpha^2}{\alpha^2-1}\right]g\right\}$$

$$\Pi_{2222} = \Pi_{3333} = \frac{3}{8(1-\nu_0)}\frac{\alpha^2}{\alpha^2-1} + \frac{1}{4(1-\nu_0)} \times \left[1 - 2\nu_0 - \frac{9\alpha^2}{4(\alpha^2-1)}\right]g$$

$$\Pi_{2233} = \Pi_{3322} = \frac{1}{4(-\nu_0)}\left\{\frac{\alpha^2}{2(\alpha^2-1)} - \left[1 - 2\nu_0 + \frac{3\alpha^2}{4(\alpha^2-1)}\right]g\right\}$$

$$\Pi_{2211} = \Pi_{3311} = -\frac{1}{2(1-\nu_0}\frac{\alpha^2}{(\alpha^2-1)} + \frac{1}{4(1-\nu_0)} \left\{\frac{3\alpha^2}{\alpha^2-1} - (1-2\nu_0)\right\}g$$

$$\Pi_{1122} = \Pi_{1133} = -\frac{1}{2(1-\nu_0)}\left\{(1-2\nu_0) + \frac{1}{\alpha^2-1}\right\} + \frac{1}{2(1-\nu_0)}\left\{(1-2\nu_0) + \frac{3}{2(\alpha^2-1)}\right\}g$$

$$\Pi_{2323} = \Pi_{3232} = \frac{1}{4(1-\nu_0)}\left\{\frac{\alpha^2}{2(\alpha^2-1)} + \left[(1-2\nu_0) - \frac{3}{4(\alpha^2-1)}\right]g\right\}$$

$$\Pi_{1212} = \Pi_{1313} = \frac{1}{4(1-\nu_0)}\left\{(1-2\nu_0) - \frac{\alpha^2+1}{\alpha^2-1} - \frac{1}{2}\left[(1-2\nu_0) - \frac{3(\alpha^2+1)}{\alpha^2-1}\right]g\right\}$$

where

$$g = \frac{\alpha}{(\alpha^2-1)^{3/2}}\{\alpha(\alpha^2-1)^{1/2} - \cosh^{-1}\alpha\}, \quad \text{prolate}$$

$$g = \frac{\alpha}{(1-\alpha^2)^{3/2}}\{\cos^{-1}\alpha - \alpha(1-\alpha^2)^{1/2}\}, \quad \text{oblate}$$